Nonlinear Single-Spin Spectrum Analyzer

Shlomi Kotler,* Nitzan Akerman, Yinnon Glickman, and Roee Ozeri

Department of Physics of Complex Systems, Weizmann Institute of Science, P. O. Box 26, Rehovot 76100, Israel

(Received 28 September 2012; revised manuscript received 21 January 2013; published 14 March 2013)

Qubits have been used as linear spectrum analyzers of their environments. Here we solve the problem of nonlinear spectral analysis, required for discrete noise induced by a strongly coupled environment. Our nonperturbative analytical model shows a nonlinear signal dependence on noise power, resulting in a spectral resolution beyond the Fourier limit as well as frequency mixing. We develop a noise characterization scheme adapted to this nonlinearity. We then apply it using a single trapped ion as a sensitive probe of strong, non-Gaussian, discrete magnetic field noise. Finally, we experimentally compared the performance of equidistant vs Uhrig modulation schemes for spectral analysis.

DOI: 10.1103/PhysRevLett.110.110503 PACS numbers: 03.67.Pp, 03.65.Yz, 42.50.Ar, 82.56.Jn

The ability of a quantum system to withstand noise is characterized by its decoherence rate: the rate at which superpositions deteriorate. Hahn's discovery [1] of the echo technique showed that decoherence can be reduced by external modulation, e.g., in the case of spins, performing a single spin flip during the experiment. Since then, the idea of using external modulation to prolong coherence, known as dynamic decoupling [2–5], has been well developed to include many pulses [6,7] and different modulation schemes [8–12].

These techniques suggested that decoherence can be used as a measurement tool. They rely on the condition that a quantum system, modulated at frequency f, is most influenced by the noise power spectral density at f [13–15]. Decoherence becomes a measure of the noise at that frequency component. If the relation between the decoherence rate and the noise power spectral density is linear, one obtains a qubit-based spectrum analyzer. This idea has been suggested in the context of different qubit technologies [16–19] and has been recently analyzed for different types of noise spectra [20]. Experimental realizations of spectral analysis through spin decoherence spectroscopy were performed with a variety of technologies including trapped ions [21,22], cold atomic ensembles [23,24], nitrogen-vacancy centers in diamonds [25], superconducting flux qubits [26], and NMR experiments in molecules [27].

The operation of such qubit spectrum analyzers fails if noise is sufficiently strong and non-Gaussian. For an experiment time T and noise amplitude N one needs to assume a small noise index $\eta \equiv NT \ll 2\pi$. If η is large, qubit evolution can be significantly nonlinear in Hamiltonian terms and the relation between measured decoherence rate and noise power is no longer linear. A straightforward remedy is to shorten the evolution time into the perturbative, linear regime. This, however, limits the frequency resolution and renders spectral analysis of strong noise impractical. In many real lab scenarios, noise is in fact too strong for its frequency components to be resolved when adhering to the linear regime.

It turns out, as will be shown in this Letter, that nonlinear spectral analysis can be performed for discrete spectra. This is reminiscent of the use of simple frequency analysis tools which enabled Babylonian astronomers to accurately predict the timings of lunar and solar eclipses [28] and 19th century scholars to provide tide predictions for various coasts and harbors [29]. This is despite the fact that nonlinear evolution is present in planet and ocean dynamics as well.

In this work we solve the problem of nonlinear qubit-based spectral analysis for discrete noise. We find a nonperturbative analytic relation between the coherence and the noise spectrum. As this relation is nonlinear, we develop a spectral estimation scheme adapted to its nonlinearity. We apply it, using a single-trapped ion, to analyze the discrete spectrum of magnetic field noise in our lab, a typical noise scenario where it is a necessity.

There are two immediate advantages of performing spectral analysis in the nonlinear limit. The first advantage is that spectral resolution supersedes the standard Fourier limit and scales as $1/(\eta T)$. For example, in this Letter we will show spectroscopy of a very strong noise ($\eta = 10$) with a Fourier limited resolution of 1.2 Hz and a nonlinear spectral resolution of 0.18 Hz. The enhancement originates from the narrowing of spectral features due to the nonlinear frequency response function. This is analogous to the narrowing of the point spread function in nonlinear microscopy. The second advantage is that if coherence is estimated by a quantum projective measurement, the optimal amplitude signal-to-(projection)noise ratio is obtained when $\eta \geq 2\pi$ (see Supplemental Material [30]).

We focus on a two-level quantum probe described by $|\psi(t)\rangle = \alpha\,|\uparrow\rangle + e^{i\phi}\beta\,|\downarrow\rangle$ and governed by a Hamiltonian $H = \hbar[N(t)\hat{\sigma}_z + \Omega(t)\hat{\sigma}_x]/2$ where $N(t)$ is classical dephasing noise and $\Omega(t)$ is the spectrum analyzer modulation. Our purpose is to use the modulation $\Omega(t)$ to

quantify the noise $N(t)$. We assume no spin relaxation processes (see Supplemental Material [30] for discussion).

For a probe initialized to $|\psi_0\rangle = (|\uparrow\rangle + |\downarrow\rangle)/\sqrt{2}$ the superposition relative phase at time T is [22],

$$\phi(T) = \int_0^T dt N(t) F(t) = \int_{-\infty}^{\infty} df N^*(f) F_T(f), \qquad (1)$$

where $F(t) \equiv \cos(\int_0^t dt' \Omega(t'))$, $N(f)$, $F_T(f)$ are the respective Fourier transforms, the latter calculated on a truncated experiment window of length T. Equation (1) is an approximation which becomes exact if $\Omega(t)$ is a train of π pulses, not necessarily equidistant (see Ref. [22]). In our experiment we used nearly ideal π pulses so Eq. (1) can be used without restriction.

Phase coherence is obtained by averaging over noise realizations, $A \equiv \langle e^{i\phi} \rangle$. The linearity of spectral analysis is based on the assumption that noise is either weak or Gaussian so that $\langle e^{i\phi} \rangle = e^{-\langle \phi^2 \rangle/2}$. In which case, the decoherence rate is indeed linearly proportional to the noise power spectral density. To calculate the phase coherence without this assumption we assume discreteness: $N(t) = \sum_{k=1}^{d} |N_k| \cos(2\pi f_k t + \alpha_k)$. For a single noise component, according to (1), $\phi = |N_0 F_T(f_0)| \cos(\alpha)$ so $\langle e^{i\phi} \rangle = (2\pi)^{-1} \int_0^{2\pi} d\alpha e^{i\phi} = J_0(|N_0 F_T(f_0)|)$ where J_0 is the zeroth Bessel function of the first kind. For an ideal sinusoidal modulation at f_0, $A = J_0(N_0 T)$. The linear limit is valid only when J_0 can be well approximated to second order in its argument. Moreover, when the noise index $\eta \equiv |N_0| T$ crosses $z_0 \approx 2.4$, the first zero of $J_0(x)$, coherence becomes negative; i.e., the superposition phase partially refocuses close to π. Such single Bessel behavior was observed with ions [22] as well as with nitrogen vacancy (NV) centers under simulated noise [31] and with a cantilever coupled to a NV center [32].

In the case of more than one noise component, the coherence behavior takes a product form over all noise components. Assuming $\alpha_k \in [0, 2\pi]$ are uniformly distributed mutually independent random variables,

$$A(T) \equiv \langle e^{i\phi} \rangle = \prod_{k=1}^{d} J_0(|N_k F_T(f_k)|). \qquad (2)$$

This equation is the main tool of our noise spectral estimation method.

The nonlinear limit also reveals frequency mixing if we allow for correlations in the α_k variables. Whenever an integer combination of the noise frequencies is nulled $\sum_k h_k f_k = 0$, additional Bessel product terms affect the coherence (see Supplemental Material [30] for derivation),

$$A(T) = \sum_{\substack{h_1,\ldots,h_d \\ \sum h_k f_k = 0 \\ \sum h_k \text{even}}} (-1)^{1/2 \sum h_k} \cos(\Sigma h_k \alpha_k) \prod_{k=1}^{d} J_{h_k}(|N_k F_T(f_k)|), \qquad (3)$$

where the h_k indices are integers and J_{h_k} the corresponding Bessel functions of first kind. The dominant summand corresponding to $h_1 = \cdots = h_d = 0$ coincides with Eq. (2). By focusing the modulation at a single frequency, as in our experiment, all the higher Bessel terms can be neglected, and information on the phase relation between different spectral components is lost. One will be able to retrieve it via the $\cos(\Sigma h_k \alpha_k)$ term by using a multitonal modulation.

The nonlinear dependance of the coherence A on the spectral filter function $F_T(f)$ implies a spectral resolution which is superior to the Fourier limit. For example, in the simple case of a single frequency component at f_0, the coherence is $A(f) = J_0\{\eta \text{sinc}[\pi(f - f_0)T]\}$. This expression can be expanded as a power series in the sinc filter function. As η increases, the coherence becomes sensitive to higher powers of the sinc function, resulting in narrower spectral features. Applying the Carmér-Rao bound [33] shows that frequency resolution scales as $1/\eta T$ as opposed to the $1/T$ scaling of Fourier limited spectroscopy (see Supplemental Material [30]).

Our system is comprised of the Zeeman submanifold of the electronic ground level of a single $^{88}Sr^+$ ion, $|\uparrow\rangle = |5s_{1/2}, J = 1/2, M_J = 1/2\rangle$ and $|\downarrow\rangle = |5s_{1/2}, J = 1/2, M_J = -1/2\rangle$. The dominant noise we measured was magnetic field fluctuations $B(t)$ due to power line harmonics rendering a discrete noise spectrum, $N(t) = g\mu_B B(t)/\hbar$, where g is the Landé g factor, μ_B the Bohr magneton and $\hbar$ the Planck constant divided by 2π [see Fig. 1(a)]. In this system, spin relaxation processes play no role (see Supplemental Material [30]). Setup details can be found in Refs. [34,35].

To measure phase coherence we performed a Ramsey-type experiment as shown in Fig. 1(b). A modulation $\Omega(t)$ of length T is sandwiched between two $\pi/2$ pulses, differing by a relative phase ϕ_{rf}. We then measured the probability of the ion to be in the $|\uparrow\rangle$ state, $P_\uparrow$, as a function of ϕ_{rf}. A fit to $P_\uparrow = \frac{1}{2} - \frac{A}{2}\cos\phi_{rf}$ yields an experimental estimate of the phase coherence A. Examples of such fringes are shown in Figs. 1(c) and 1(d). In all cases, $\Omega(t)$ was a train of π pulses at different times and possibly different rotation axes.

A first distinctive characteristic of nonlinearity is the negative values of the coherence (noise index $\eta > z_0$), shown in Fig. 1(e). Here we fixed the modulation frequency at $f_{\text{mod}} = 100$ Hz while increasing n, the number of equidistant pulses. As seen, the fringe contrast with $n = 19$ [shown in Fig. 1(d)] is inverted with respect to $n = 1$ [shown in Fig. 1(c)]. A fit to Eq. (2) is shown by the red line, assuming a single spectral component at 100 Hz, with N_0 as a single fit parameter and results in $B_{100\text{ Hz}} = 3.0(2)\ \mu$G. Physically, negative coherence values result from rephasing of spins when the standard deviation of phase accumulation due to noise becomes roughly π. This is a signature of the topology of spins state space, which limits the spin trajectory to a sphere.

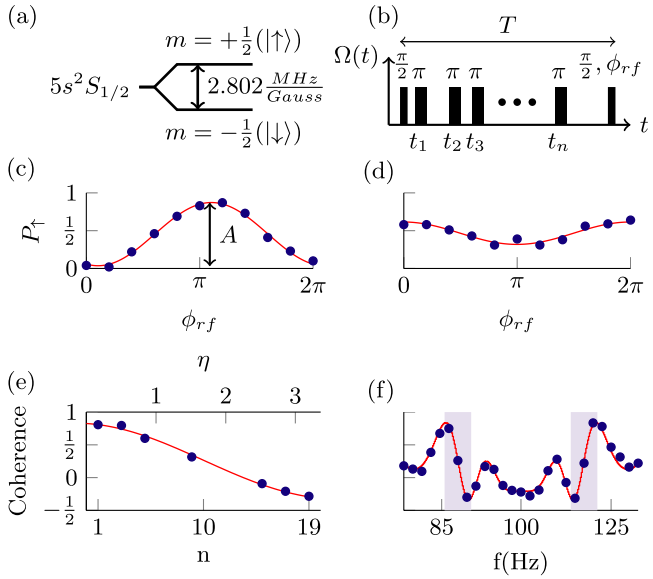

FIG. 1 (color online). (a) $^{88}Sr^+$ ground state manifold comprising the Zeeman sensitive quantum probe. (b) Typical experimental sequence with n modulation pulses sandwiched between two $\pi/2$ pulses with a relative ϕ_{rf} phase. (c), (d) Probability of finding the probe in the $|\uparrow\rangle$ state at the end of a sequence vs the rf relative phase. Red line is a best fit to $P_\uparrow = 1/2 - A/2\cos(\phi_{rf})$, A is the coherence. (e) Nonlinear response of the coherence with respect to the number of equidistant pulses n. Interpulse distance was 5 ms. The first and last points correspond to the fringes in 1(c) and 1(d), respectively. Red line is a single parameter best fit to Eq. (2). Inversion of the fringe contrast in (d) corresponds to negative coherence. (f) Nonlinear response of the coherence with respect to modulation frequency, with $n = 11$ equidistant pulses. Spectrum corresponds to a single, highly nonperturbative noise component. Spectral features, narrower than the Fourier resolution, are highlighted by the shaded regions. These features are 4 Hz FWHM whereas the Fourier limit is 17 Hz. Red line is a single parameter best fit to Eq. (2).

A second mark of nonlinearity is that multiple spectral features can arise from a single noise component, as shown in Fig. 1(f). The number of pulses is fixed at $n = 11$ and the modulation frequency is scanned across $f = 100$ Hz. The spectrum shows five coherence minima. Unlike the linear case, these do not correspond to five different spectral components but rather to a broadened response to a magnetic field monotone. Again, a fit to Eq. (2) with N_0 as a single fit parameter is shown by the red line and yields $B_{100\ \mathrm{Hz}} = 15.3(3)\ \mu$G. This noise amplitude corresponds to a noise index of $\eta = 10.3(2)$, well in the strong noise regime. The noise amplitudes extracted from the data shown in Figs. 1(e) and 1(f) are very different as these data sets were taken at different times.

A third feature of the nonlinear regime is the superior-to-Fourier frequency resolution. This is well demonstrated in the data displayed in Fig. 1(f). The Fourier limit suggests that the 100 Hz decoherence feature should not be narrower than $1/T = 17$ Hz. However, the features marked by the shaded stripes in Fig. 1(f) have a full width at half maximum (FWHM) of 4 Hz indicating spectral narrowing due to nonlinearity. For $r = 200$ experiment repetitions the Fourier limited resolution is $1/T\sqrt{r} = 1.2$ Hz. With the nonlinear gain we expect a resolution of $1/\eta T\sqrt{r} = 0.12$ Hz. Indeed, if the noise frequency f_0 is allowed to vary, a best fit to the points of steepest inclination (two central points of the shaded region in Fig. 1, total of $r = 200$ repetitions) yields $f_0 = 100 \pm 0.18$ Hz, in reasonable agreement with the theoretical bound. The ability to distinguish between two noise components also benefits from the nonlinear gain in resolution. This is discussed in the Supplemental Material [30] where we develop an analog to the Rayleigh criteria in optics.

To practically estimate a multitone discrete spectrum we first identify the frequencies f_k of its components. In any modulation scheme, the peak of the modulation $F_T(f)$ increases linearly with the total experiment time T while improving spectral resolution. To identify the different noise components we therefore modulated the probe at different frequencies. For each modulation frequency the number of pulses was increased until the different noise components emerged. Examples are shown in Figs. 2(a) and 2(b). The two data sets were measured four months apart with a different magnetic environment; the spectral response at 150 Hz which is clear in Fig. 2(a) almost vanished in Fig. 2(b) where a new 200 Hz component appeared.

Once the component frequencies $\{f_k\}$ have been determined, the multiplicative structure of Eq. (2) is used to determine their magnitudes N_k. Whenever the coherence $A(T)$ crosses zero, with high probability, only one of the Bessel functions in the product is nulled. If the modulation

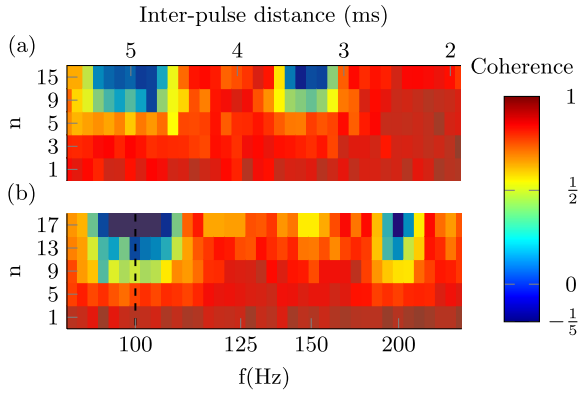

FIG. 2 (color online). Spectral peak identification adapted to the nonlinear regime. Two scans taken several months apart. Each scan is a color map of coherence vs the number of pulses n and the modulation frequency. The upper scan shows clear features at 100 and 150 Hz. The latter nearly vanishes in the lower scan and a new 200 Hz component appears. The crossing from positive to negative coherence marked by the dashed line in (b) can be used to extract the noise magnitude at 100 Hz as described in the text.

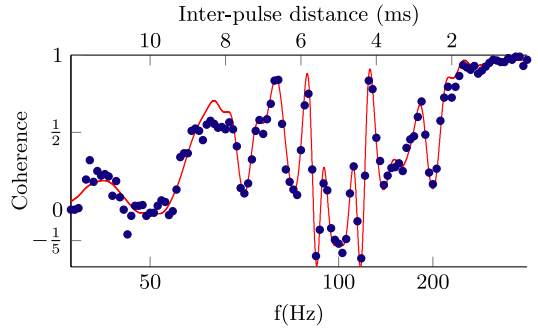

FIG. 3 (color online). Fine-tuning of noise magnitudes in the nonlinear regime. Once noise components have been identified in frequency and magnitude, a fine-tuning estimate is obtained by scanning the modulation frequency and fitting to the full spectrum to Eq. (2) (red line). Here we use an $n = 11$ equidistant pulse sequence. Nonlinearity is well pronounced around $f = 100$ Hz where it renders spectral features narrower than the Fourier limit with almost a tenfold improvement in spectral resolution, as discussed in the text.

is centered about f_k, increasing the experiment time T until the first zero crossing occurs implies that the corresponding Bessel has been nulled and provides an estimate for N_k. For example, from the zero crossing encountered along the dashed marked column in Fig. 2(b) we obtain a zero crossing estimate of 2.6(2) μG for the noise amplitude at 100 Hz.

The last stage of spectral characterization is fine-tuning of the estimated noise magnitudes with a full fit procedure, using the previously estimated field magnitudes as a starting point. Such a fit to Eq. (2) is shown in Fig. 3 with five fit parameters $B_{50\ \mathrm{Hz}} = 2.0(1)\ \mu$G, $B_{100\ \mathrm{Hz}} = 15.4(4)\ \mu$G, $B_{150\ \mathrm{Hz}} = 4.2(3)\ \mu$G, $B_{200\ \mathrm{Hz}} = 6.3(3)\ \mu$G, and a slowly varying field, $(g\mu_B B_{\mathrm{slow}}/h) f_{\mathrm{slow}} = 66(2)\ \mathrm{Hz}^2$. The nonperturbative nature of the spectrum is quantified by the corresponding noise indices: $\eta_{50} = 2.7(1)$, $\eta_{100} = 10.4(3)$, $\eta_{150} = 1.9(1)$, $\eta_{200} = 2.1(1)$.

What modulation is best suited for spectrum estimation? For the purpose of noise spectroscopy Yuge *et al.* [20] suggested an equidistant pulse scheme while Cywiński *et al.* [17] suggested the Uhrig [9] scheme. A comparison of typical modulation spectra of the two is shown in the insets of Figs. 4(c) and 4(d); in both cases the total experiment time is $T = 66.7$ ms.

The interpretational simplicity of equidistant modulation is pronounced in the two-dimensional scan shown in Fig. 4(a). For each fixed experiment duration, T, a phase scan is shown as a column in Fig. 4(a). The contrast of each column is obtained from a fit procedure and displayed as a single data point in Fig. 4(c), correspondingly. The noise spectral peaks can be easily identified at 150, 200, and 250 Hz. The spectral shape of the Uhrig modulation [inset of Fig. 4(d)] convolutes nearby frequency components of the noise, as seen in Figs. 4(b) and 4(d).

Quantitatively, with our noise profile, both modulation schemes performed equally well [Figs. 4(c) and 4(d)] and show agreement in the extracted spectrum below 1 standard deviation as detailed in the Supplemental Material [30].

The theory and technique described in this Letter were indispensable in measuring our lab noise characteristics. It enabled us to calibrate our magnetic field compensation system and reduce noise components to the μG level [22]. We expect this model to be useful for other discrete strong noise scenarios. One example is spontaneous α oscillations in brain activity measured using magnetoencephalography [36]. Another example is the study of decoherence of a single NV center induced by a finite number of ^{13}C nuclear

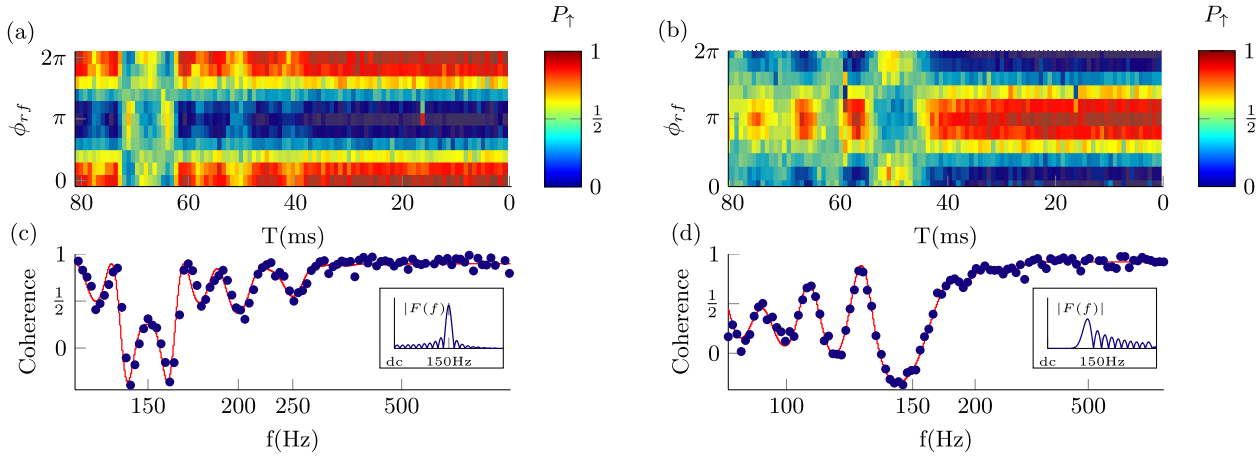

FIG. 4 (color online). Comparison of equidistant vs Uhrig modulation. (a) Each column is a scan of ϕ_{rf} at $n = 19$ equidistant pulses and a fixed T. The total experiment time T is varied from column to column and the corresponding contrast and modulation frequency is shown in (c). (b) Same as (a), for an Uhrig scheme of 20 pulses. (c) Red line is a fit to Eq. (2). (d) Same as (c), for the Uhrig scheme. The fit indicated by the red line yields field magnitudes consistent with the equidistant modulation fit in (c). Inset in (c) shows the spectrum of equidistant modulation with 19 pulses and a total duration of 66.7 ms. Inset in (d) is the same as the inset in (c) for Uhrig modulation with 20 pulses.

spins in diamond [37] or the discrete mechanical resonances of a cantilever coupled to a NV center [32].

We gratefully acknowledge the support by the Israeli Science Foundation, the Minerva Foundation, the German-Israeli Foundation for Scientific Research, the US-Israel Binational Science Foundation, the Crown Photonics Center, David Dickstein, France, and Martin Kushner Schnur, Mexico.

*shlomi.kotler@weizmann.ac.il; www.weizmann.ac.il/complex/ozeri

[1] E. L. Hahn, Phys. Rev. **80**, 580 (1950).
[2] L. Viola and S. Lloyd, Phys. Rev. A **58**, 2733 (1998).
[3] M. Ban, J. Mod. Opt. **45**, 2315 (1998).
[4] L. Viola, E. Knill, and S. Lloyd, Phys. Rev. Lett. **82**, 2417 (1999).
[5] D. Vitali and P. Tombesi, Phys. Rev. A **59**, 4178 (1999).
[6] H. Y. Carr and E. M. Purcell, Phys. Rev. **94**, 630 (1954).
[7] S. Meiboom and D. Gill, Rev. Sci. Instrum. **29**, 688 (1958).
[8] K. Khodjasteh and D. A. Lidar, Phys. Rev. Lett. **95**, 180501 (2005).
[9] G. S. Uhrig, Phys. Rev. Lett. **98**, 100504 (2007).
[10] G. Gordon, G. Kurizki, and D. A. Lidar, Phys. Rev. Lett. **101**, 010403 (2008).
[11] H. Uys, M. J. Biercuk, and J. J. Bollinger, Phys. Rev. Lett. **103**, 040501 (2009).
[12] J. Clausen, G. Bensky, and G. Kurizki, Phys. Rev. Lett. **104**, 040401 (2010).
[13] A. G. Kofman and G. Kurizki, Phys. Rev. Lett. **87**, 270405 (2001).
[14] A. G. Kofman and G. Kurizki, Phys. Rev. Lett. **93**, 130406 (2004).
[15] G. Gordon, N. Erez, and G. Kurizki, J. Phys. B **40**, S75 (2007).
[16] S. Lasic, J. Stepisnik, and A. Mohoric, J. Magn. Reson. **182**, 208 (2006).
[17] L. Cywiński, R. M. Lutchyn, C. P. Nave, and S. Das Sarma, Phys. Rev. B **77**, 174509 (2008).
[18] R. de Sousa, in *Electron Spin Resonance and Related Phenomena in Low-Dimensional Structures*, edited by M. Fanciulli, Topics in Applied Physics, Vol. 115 (Springer, Berlin, Heidelberg, 2009), pp. 183220.
[19] L. T. Hall, J. H. Cole, C. D. Hill, and L. C. L. Hollenberg, Phys. Rev. Lett. **103**, 220802 (2009).
[20] T. Yuge, S. Sasaki, and Y. Hirayama, Phys. Rev. Lett. **107**, 170504 (2011).
[21] M. J. Biercuk, H. Uys, A. P. VanDevender, N. Shiga, W. M. Itano, and J. J. Bollinger, Nature (London) **458**, 996 (2009).
[22] S. Kotler, N. Akerman, Y. Glickman, A. Keselman, and R. Ozeri, Nature (London) **473**, 61 (2011).
[23] Y. Sagi, I. Almog, and N. Davidson, Phys. Rev. Lett. **105**, 053201 (2010).
[24] I. Almog, Y. Sagi, G. Gordon, G. Bensky, G. Kurizki, and N. Davidson, J. Phys. B **44**, 154006 (2011).
[25] G. de Lange, Z. H. Wang, D. Rist, V. V. Dobrovitski, and R. Hanson, Science **330**, 60 (2010).
[26] J. Bylander, S. Gustavsson, F. Yan, F. Yoshihara, K. Harrabi, G. Fitch, D. G. Cory, Y. Nakamura, J.-S. Tsai, and W. D. Oliver, Nat. Phys. **7**, 565 (2011).
[27] G. A. Álvarez and D. Suter, Phys. Rev. Lett. **107**, 230501 (2011).
[28] O. Neugebauer, *The Exact Sciences in Antiquity* (Courier Dover Publications, Mineola, NY, 1969).
[29] B. Parker, Phys. Today **64**, No. 9, 35 (2011).
[30] See Supplemental Material at http://link.aps.org/supplemental/10.1103/PhysRevLett.110.110503 for analytic theory of the nonlinear spectrum analyzer, implications on frequency resolution and frequency mixing, quantitative comparison of Uhrig vs equidistant modulation.
[31] A. Laraoui, J. S. Hodges, and C. A. Meriles, Appl. Phys. Lett. **97**, 143104 (2010).
[32] S. Kolkowitz, A. C. Bleszynski Jayich, Q. P. Unterreithmeier, S. D. Bennett, P. Rabl, J. G. E. Harris, and M. D. Lukin, Science **335**, 1603 (2012).
[33] C. R. Rao, Bull. Calcutta Math. Soc. **37**, 81 (1945).
[34] N. Akerman, Y. Glickman, S. Kotler, A. Keselman, and R. Ozeri, Appl. Phys. B **107**, 1167 (2012).
[35] A. Keselman, Y. Glickman, N. Akerman, S. Kotler, and R. Ozeri, New J. Phys. **13**, 073027 (2011).
[36] T. H. Sander, J. Preusser, R. Mhaskar, J. Kitching, L. Trahms, and S. Knappe, Biomed. Opt. Express **3**, 981 (2012).
[37] F. Reinhard, F. Shi, N. Zhao, F. Rempp, B. Naydenov, J. Meijer, L. T. Hall, L. Hollenberg, J. Du, R.-B. Liu, and J. Wrachtrup, Phys. Rev. Lett. **108**, 200402 (2012).